Prolonged activity of a recombinant manganese superoxide dismutase through a formulation of polymeric multi-layer nanoassemblies targeting cancer cells.

Giacomo Russo[1$*], Giulia Iaccarino[2$], Marialuisa Piccolo[3], Maria Grazia Ferraro[3], Raffaele Vecchione[2*], Lucia Grumetto[4,5*], Paolo A. Netti[2**], Rita Santamaria[3,5**]

1. School of Applied Sciences, Sighthill Campus, Edinburgh Napier University, 9 Sighthill Ct, EH11 4BN Edinburgh, United Kingdom.

2. Center for Advanced Biomaterials for Health Care@CRIB, Istituto Italiano di Tecnologia, Largo Barsanti e Matteucci 53, Naples 80125, Italy

3.BioChem Laboratory, Department of Pharmacy, School of Medicine and Surgery, University of Naples Federico II, Via D. Montesano, 49, I-80131 Naples, Italy

4.Pharm-Analysis & Bio-Pharm Laboratory, Department of Pharmacy, School of Medicine and Surgery, University of Naples Federico II, Via D. Montesano, 49, I-80131, Naples, Italy.

5. Consorzio Interuniversitario INBB, Viale Medaglie d'Oro, 305, I-00136, Rome, Italy

[$]These authors equally contributed to the work.

*Corresponding author

** Last author

To whom correspondence should be addressed:

Prof. Lucia Grumetto, Pharm-Analysis & Bio-Pharm Laboratory, Department of Pharmacy, School of Medicine and Surgery, University of Naples Federico II, Via D. Montesano, 49, I-80131, Naples, Italy Electronic mail: grumetto@unina.it, Telephone: +39 081678628, Fax +39 081678107.

Dr. Giacomo Russo, School of Applied Sciences, Edinburgh Napier University, Sighthill Campus Edinburgh, UK. Electronic mail: G.Russo@napier.ac.uk, Telephone: +44 (0) 131 455 3464, Fax +44 (0) 131 455 3555

Dr. Raffaele Vecchione, Center for Advanced Biomaterials for Health Care@CRIB, Istituto Italiano di Tecnologia, Largo Barsanti e Matteucci 53, Naples 80125, Italy, Electronic mail: Raffaele.Vecchione@iit.it Telephone: +3908119933127, Fax +3908119933140

Prolonged activity of a recombinant manganese superoxide dismutase through a formulation of polymeric multi-layer nanoassemblies targeting cancer cells.

Giacomo Russo[1$*], Giulia Iaccarino[2$], Marialuisa Piccolo[3], Maria Grazia Ferraro[3], Raffaele Vecchione[2*], Lucia Grumetto [4,5*], Paolo A. Netti[2**], Rita Santamaria[3,5**]

1. School of Applied Sciences, Sighthill Campus, Edinburgh Napier University, 9 Sighthill Ct, EH11 4BN Edinburgh, United Kingdom.

2. Center for Advanced Biomaterials for Health Care@CRIB, Istituto Italiano di Tecnologia, Largo Barsanti e Matteucci 53, Naples 80125, Italy

3.BioChem Laboratory, Department of Pharmacy, School of Medicine and Surgery, University of Naples Federico II, Via D. Montesano, 49, I-80131 Naples, Italy

4.Pharm-Analysis & Bio-Pharm Laboratory, Department of Pharmacy, School of Medicine and Surgery, University of Naples Federico II, Via D. Montesano, 49, I-80131, Naples, Italy.

5. Consorzio Interuniversitario INBB, Viale Medaglie d'Oro, 305, I-00136, Rome, Italy

[$]These authors equally contributed to the work.

*Corresponding author

** Last author

Graphical abstract

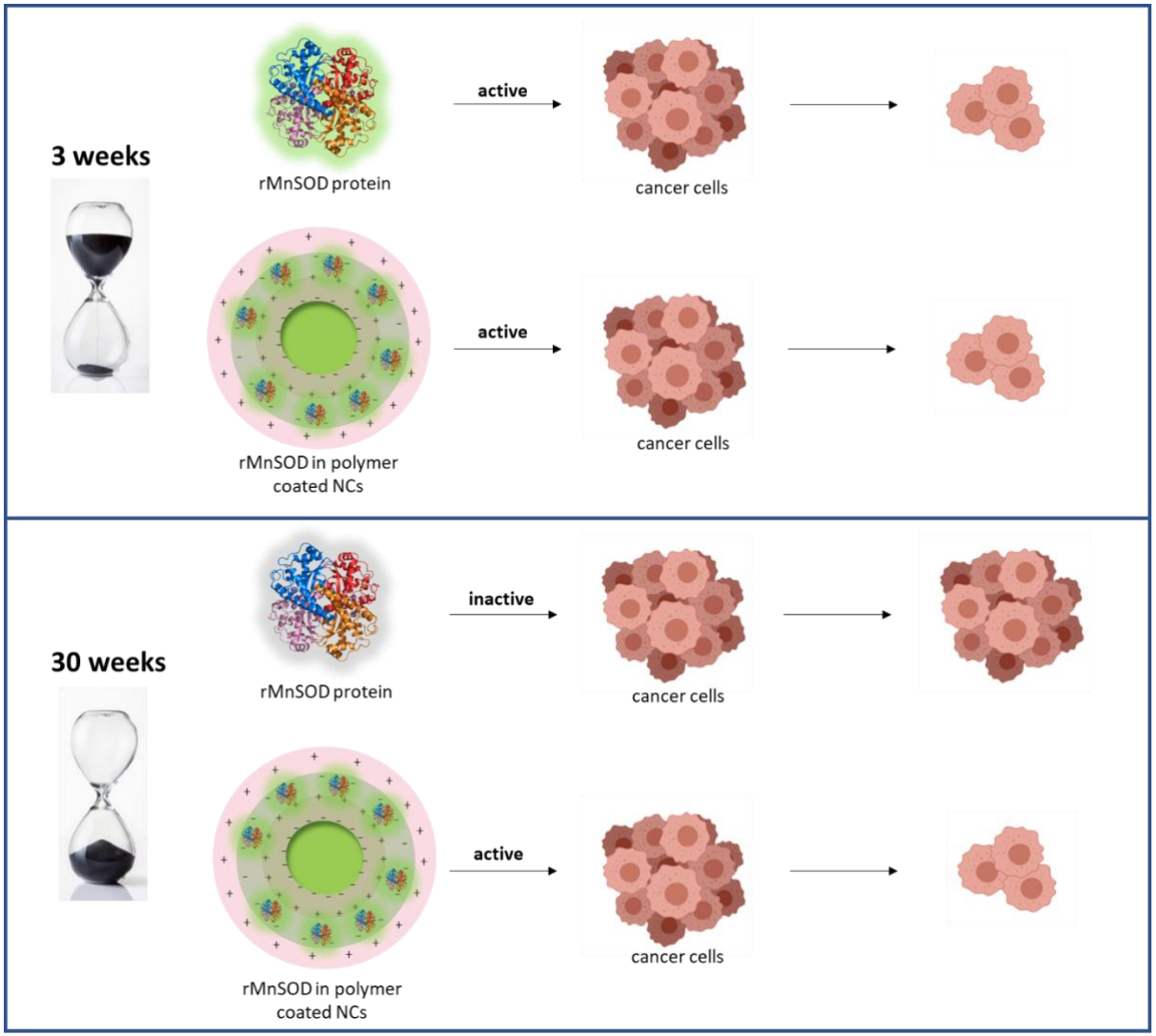

Abstract

A new isoform of human manganese superoxide dismutase (SOD) has been recently isolated and obtained in a synthetic recombinant form and termed rMnSOD. As compared to other SODs, this isoform exhibits a dramatically improved cellular uptake and an intense antioxidant and antitumoral activity. Unfortunately, its use is severely hampered as this active pharmaceutical ingredient (API) in solution suffers from remarkable instability, which realizes as an interplay of unfolding and aggregation phenomena. This leads the API to be ineffective after three weeks only when stored at 4 °C.

A formulation strategy was undertaken to mitigate this instability. This was based on the incorporation of the API in hyaluronic acid and its layer-by-layer deposition over a chitosan-n-acetyl cysteine- monolayer nanoemulsion (NE) and its subsequent coverage with a further external interface of a chitosan-n-acetyl cysteine. The obtained constructs were tested over a selected panel of healthy and cancerous cell lines. The undertaken formulation strategy enhanced the API's effect and selectivity *in vitro* already at time zero, maintaining and extending the efficacy of this anticancer agent until up to 30 weeks when stored at 4°C.

Keywords: Superoxide dismutase; cancer cells; antiproliferative effect; protein stability; nanocarrier; layer-by-layer deposition; nanofabrication.

1. Introduction

Although over a hundred recombinant proteins are clinically used as therapeutic agents, their massive implementation is nowadays severely hampered by their remarkable physical and chemical instability, which affect the shelf-life, thus the efficacy, of most of these active pharmaceutical ingredients (APIs) (Krause and Sahin, 2019).

Superoxide dismutases (SODs)(Holley et al., 2011) are ubiquitous antioxidant metalloenzymes catalyzing the O_2^- free radical dismutation of hydrogen peroxide (H_2O_2). Their action prevents the accumulation of these reactive oxygen species (ROS), which detrimentally affect cellular

homeostasis leading in some cases to cancer development. At least three types of SODs are present in human tissues, including cytoplasmic Cu/Zn-SOD, extracellular Cu/Zn-SOD, and mitochondrial manganese (Mn) SOD (MnSOD). The isoform 2 of this manganese-dependent MnSOD-2 is characteristic of aerobic organisms and is composed of four homologous 24-kDa subunits (Holley et al., 2011). MnSOD-2 is synthesized in the cytoplasm and then driven into the mitochondrial matrix *via* its leader sequence, consisting of 24 amino acids. This peptide is subsequently cleaved, resulting in a mature and enzymatically active protein that plays a fundamental role within the cell. SODs appear to control multiple reactions, essential to the determination of cell fate, particularly for cancer cells (Folz et al., 1997; Wan et al., 1994). Unfortunately, none of the commercially available SODs can enter cells and, consequently, they are rapidly inactivated or eliminated from the blood stream.

A new isoform of human MnSOD was isolated and obtained in a synthetic recombinant form and termed rMnSOD (Borrelli et al., 2009; Mancini et al., 2008; Mancini et al., 2006). This isoform differs from the others because of its capability to enter cells by means of its uncleaved 24-aa leader peptide which acts as a molecular carrier and its intense antioxidant and antitumor activity. rMnSOD appears to be very effective at O_2– scavenging both intra- and extracellularly and at improving pathological conditions associated with increased oxidative stress. rMnSOD also provides protection to rat kidneys treated with cyclosporine A, allowing for the recovery of 80% of their glomerular filtrate (Damiano et al., 2013). Moreover, rMnSOD is radio protective for healthy cells (Grumetto et al., 2015) and radiosensitive for cancer cells and displays a specific and selective cytotoxic activity against tumour cells overexpressing the estrogenic receptor (ER) (Borrelli et al., 2009; Ceelen and Flessner, 2010; Greenlee et al., 2000; Momenimovahed et al., 2019; Ye et al., 2015; Zhidkov et al., 2013) like ovarian cancer that is currently one of the greatest clinical challenges in gynecologic oncology (Greenlee et al., 2000; Momenimovahed et al., 2019).

Unfortunately, rMnSO, as protein, is extremely unstable in water solution, especially when exposed to environmental light, temperature and humidity (Krause and Sahin, 2019). In this work we propose a strategy to enhance the API shelf life by creating polymer multilayer nano-assemblies aimed at preventing aggregation and unfolding mechanisms. We show two possible configurations of layer-by-layer nanocapsules (NCs) differing in their external layer, which is hyaluronic acid in one case (thereafter referred to as rMnSOD bilayer NCs) and

chitosan-n-acetylcysteine in another case (thereafter referred to as rMnSOD trilayer NCs). The latter design is meant for a superior residence time in the cancerous lesion thanks to its well-known mucoadhesive properties(Vecchione et al., 2014) laying the foreground to a sustained delivery *in situ*. The second configuration is meant for the active targeting towards cancer cells by a molecular recognition of the cluster of differentiation 44 (CD44)(Vecchione et al., 2016), a ubiquitously glycoprotein present on the surface of most mammalian cells and over-expressed in a variety of solid tumours.

We investigated the biological activity of the naked rMnSOD and colloidal suspension of the nano-encapsulated API on a selected panel of cell lines in standard storage conditions to evaluate their effect on cell viability at different times after their fabrication.

2. Materials and Methods

2.1 Materials

Both soybean oil (density at 20 °C of 0.922 g/mL) and surfactant Lipoid E80 (egg lecithin powder 80%–85% enriched with phosphatidyl choline (PC) and 7%–9.5% content in phosphatidyl ethanolamine (PE)) were purchased from Lipoid (Ludwigshafen, Germany) and used without further purification. Millipore Milli-Q water (resistivity of 18.2 MΩ.cm (at 25°C) and a TOC value below 5 ppb) was used for the preparation of all formulations. Glacial acetic acid, chitosan-n-acetylcysteine (CT-NAC) (LMW 190 kDa) and Hyaluronic acid sodium salt from bovine vitreous humor were purchased from Sigma Aldrich (Milan, Italy). A 1 mg/mL stock solution of rMnSOD in Milli Q water was generously donated by Prof. Aldo Mancini, Istituto Nazionale Tumori IRCCS Fondazione G. Pascale, Naples, Italy. This solution was kept at -20 °C long term storage, and at 4 °C for daily use.

2.2 Formulation: design and development

The preparation of primary emulsions that represented the starting point for sub sequential polymer network coating was accomplished as already described in (Vecchione et al., 2014) and further expanded in (Vecchione et al., 2016).

The progressive deposition of alternating layers of polyelectrolyte polymers was carefully checked by constant measurements of particle size and ζ-potential of the diluted suspensions. Nanoemulsions featuring standard deviation greater than 5% in both parameters were discarded. The deposition took place as detailed elsewhere(Vecchione et al., 2016). The nano assemblies were fabricated by aid of two syringe pumps (HARVARD APPARATUS 11 PLUS, Holliston, Massachusetts, USA) and an ultrasonic bath (FALC INSTRUMENTS, Treviglio (BG), Italy). In particular, a secondary nanoemulsion, based on an oil concentration of 14 % (v:v), was mixed 1:1 (v:v) with and a 0.14 % CT-NAC solution in a 20 mM acetic acid solution. This was prepared by weighting 10.0 mg of CT-NAC, which was slowly dissolved in 20 mL of a 100 mM acetic acid solution in Milli Q water under gentle magnetic stirring. The two liquid phases were injected simultaneously at the same flow rate (0.4 mL/min) through two micrometric capillaries interfaced at their extremities (force level 80%). Due to the high surface tension, each microvolumes released from the two capillaries coalesced to form one drop containing the very first instants of the deposition process. Each drop of the infused solution was then collected at the bottom of a glass tube, avoiding that any contact between sample and the glass wall took place. The glass tube was immersed in the ultra-sonic bath at room temperature, a frequency of 59 kHz and 100% power for the whole duration of the deposition process, *i.e.,* until all the volumes of both working solutions poured out from both syringes. Subsequently, the same syringe pump set up was used to stratify and incorporate the rMnSOD in a hyaluronic acid network *via* deposition of a 0.048% (w/w) hyaluronic acid and a 0.012% (w/w) rMnSOD aqueous solution, which were again mixed 1:1.

This mixture was then deposited on the monolayer assemblies previously fabricated and led to the fabrication of rMnSOD bilayer NCs. The final step implied the coating of the nano-assemblies with an external shell of CT-NAC by mixing equal volumes (500 µL) of a 0.018 % (w:w) CT-NAC in 20 mM acetic acid and the bilayer NCs previously fabricated, thus achieving rMnSOD trilayer NCs.

2.3 Characterization of the nano assemblies

Size distribution and ζ-potential of all the suspensions were measured by Zeta- sizer (NanoSeries, Malvern, Malvern, Worcestershire, United Kingdom) using the laser Dynamic Light Scattering (DLS) (λ = 632.8 nm) and particle electrophoresis techniques, respectively.

All the suspensions were diluted to a droplet concentration of approximately 0.025 (wt%), using Milli-Q water in the case of primary nanoemulsions and nanocapsules terminating with hyaluronic acid, and acetic acid Milli-Q water solution (pH 4, 6.5 × 10−4 M) for nanocapsules terminating with CT-NAC. A default refractive index ratio (1.52) and five runs for each measurement (one run lasting 100 s) were used in the calculations of the particle size distribution.

ζ-potential measurements of macroparticles able to scatter optical light are standard and validated (Stetefeld et al., 2016). Prior to analysis, all the suspensions were diluted in the same conditions as for the size measurement. 50 runs for each measurement were set to carry out the ζ-potential analysis.

2.4 Electron cryotomography (CryoET) characterization

The morphology of the secondary nanomulsions and multilayer nanocapsules were observed by cryo-EM. Frozen hydrated samples were prepared by applying a 3 µL aliquot to a previously glow-discharged 200 mesh holey carbon grids (Ted Pella, USA). Before plunging into nitrogen cooled liquid ethane, the grid was blotted for 1.5 s in a chamber at 4 °C and 90% humidity using a FEI Vitrobot Mark IV (FEI company, the Netherlands). The particles were imaged using a Tecnai G2 F20 transmission electron microscope (FEI company, the Netherland) equipped with a Schottky field emission gun operating at an acceleration voltage of 200 kV and recorded at low dose with a 2 k × 2 k Ultrascan (Gatan, USA) CCD camera.

2.5 Scanning Electron Microscopy (SEM)

For SEM measurements a small amount of solution containing nanocapsules was dropped onto the surface of an aluminum stub covered by a glass plate. The sample was then sputter-coated with a thin Pt/Pd or gold layer (10 nm) in a Cressington sputter coater 208 HR. The aluminum stub containing the Pt/Pd or gold – coated sample was then placed in a FEG-SEM

198 scanning electron microscope and imaged using 20 kV accelerating voltage. For imaging
199 analysis of cells, samples were first fixed with a sodium cacodylate 0.1 M in glutaraldehyde
200 solution (2.5% wt) at room temperature for 2 h. The sample was then washed with a solution
201 of 0.1 M sodium cacodylate – 0.1 M sucrose (3 times in an ice bath for 10 min). Samples were
202 then fixed with OsO4 (1% wt. in 0.1 M sodium cacodylate – 0.1 M sucrose) and washed again
203 with a solution of 0.1 M sodium cacodylate – 0.1 M sucrose (3 times in an ice bath for 10 min).
204 In the end samples were dehydrated by replacing the water solution with a series of ethanol
205 solutions (30%, 50%, 75%, 95%, 95%, 100%, 100%, 100% (v/v)) and dried with a Critical Point
206 Drier (Leica EM CPD300). As for NCs, the samples were then sputter-coated and imaged as
207 previously described.

208

209 *2.6 Cell cultures*

210 Epithelial-like type human breast adenocarcinoma cells MCF-7 (Endocrine-Responsive, ER)
211 and human HaCaT keratinocytes were grown in DMEM (Invitrogen, Paisley, UK)
212 supplemented with 10% fetal bovine serum (FBS, Cambrex, Verviers, Belgium), L-glutamine
213 (2 mM, Sigma Aldrich, Milan, Italy), penicillin (100 units/mL, Sigma Aldrich) and streptomycin
214 (100 µg/mL, Sigma Aldrich). Human ovarian carcinoma cells A2780 were grown in RPMI 1640
215 medium (ATCC modification) supplemented with 10% fetal bovine serum (FBS, Cambrex,
216 Verviers, Belgium), L-glutamine (2 mM, Sigma Aldrich, Milan, Italy), penicillin (100 units/mL,
217 Sigma Aldrich) and streptomycin (100 µg/mL, Sigma Aldrich, Milan, Italy). MCF 10A, a non-
218 tumorigenic mammary gland epithelial cell line, was maintained in DMEM (Invitrogen,
219 Carlsbad, CA) supplemented with 5% horse serum (Invitrogen, Carlsbad, California, USA), 500
220 ng/mL hydrocortisone (Sigma-Aldrich, St. Louis, MO), 100 ng/mL cholera toxin (Sigma-Aldrich,
221 Milan Italy), 10 µg/mL insulin (Invitrogen, Carlsbad, California, USA), 20 ng/mL epidermal
222 growth factor (EGF, Sigma Aldrich, Milan, Italy), penicillin (100 units/mL, Sigma Aldrich, Milan,
223 Italy) and streptomycin (100 µg/mL, Sigma Aldrich, Milan, Italy). All cell lines have been
224 cultured in a humidified 5% carbon dioxide atmosphere at 37 °C. MCF-10A and A2780 cell
225 lines were generously donated by Dr. Antonella Borelli, Istituto Nazionale Tumori IRCCS
226 Fondazione G. Pascale, Naples, Italy.

227

2.7 Bioscreens in vitro

The cytotoxic effects of blank formulation, the rMnSOD either formulated in NCs or solubilized in aqueous solution were investigated through the estimation of a "cell survival index", arising from the combination of cell viability evaluation with cell counting, as previously reported (Piccolo et al., 2019b). The cell survival index was calculated as the arithmetic mean between the percentage values derived from the MTT assay and the automated cell count. Cells were inoculated in 96-microwell culture plates at a density of 10^4 cells/well and allowed growing for 24 h. The medium was then replaced with fresh medium and cells were treated for additional 48 h with blank formulation, the formulated and not formulated rMnSOD. Cell viability was evaluated using the MTT assay procedure as previously described (Piccolo et al., 2019a) Cell number was determined by TC20 automated cell counter (Bio-Rad, Milan, Italy), providing an accurate and reproducible total count of cells and a live/dead ratio in one step by a specific dye (trypan blue) exclusion assay. The calculation of the concentration required to inhibit the net increase in the cell number and viability by 50% (IC_{50}) is based on plots of data (n = 6 for each experiment) and repeated five times (total n = 30). IC_{50} values were calculated from a dose response curve by nonlinear regression using a curve fitting program, GraphPad Prism 7.0, and are expressed as mean values ± SEM (n = 30) of five independent experiments.

2.8 Statistical Analysis

All data were presented as mean values ± SEM. The statistical analysis was performed using Graph-Pad Prism (Graph-Pad software Inc., San Diego, CA) and ANOVA test for multiple comparisons was performed followed by Bonferroni's test.

3. Results and Discussion

3.1 Characterization and effects of naked rMnSOD

As previously stated, while the wild-type SOD constitutively expressed in the mitochondrial matrix cannot permeate cells, the rMnSOD is effectively up taken by means of its 24 AA leader

peptide (Borrelli et al., 2016). A high degree of sequence homology between these two forms has been observed, leading to an overlap of their enzymatic activities. However, sequence heterology is instead responsible not only of rMnSOD cell's internalization, but also of a superior liability of this protein to undergo chemical and physical instability, negatively affecting pre-formulative expedients to improve its activity. In fact, circular dichroism experiments (Mancini et al., 2008) indicate that the unfolding temperature for rMnSOD is 59 °C, which stands about 30 °C below that of the wild-type SOD. At this temperature, the protein undergoes permanent unfolding, which precedes irreversible aggregation. The decreased thermal stability of rMnSOD with respect to the wild-type protein suggests that the subunit fold is heavily destabilized because of both the insertion of the leader peptide at the N-terminus and the sequence of the binding sites accommodating metal ions. Nevertheless, both these elements are essential for a possible implementation of rMnSOD as therapeutic agent due to its demonstrated antiproliferative effect on cancerous cells expressing estrogenic receptor (ER) (Borrelli et al., 2016). Before setting any endpoints, we studied the activity of unformulated rMnSOD, stored at 4°C, over a 10-weeks period. A 0.985 µM rMnSOD aqueous solution was tested on a selected panel of healthy and cancerous cell lines at fixed time ranges under the experimental conditions described in 2.2 and the results are reported in Figure 1.

At t_0 the rMnSOD exerts an antiproliferative effect on cancerous cell lines, *i.e.* A2780 and MCF-7, being generally less cytotoxic on healthy cell line, *i.e.,* HaCaT. The antiproliferative effect of rMnSOD on MCF10A cells was previously evaluated, showing no significant cytotoxic effect (Mancini et al., 2006). However, rMnSOD effectiveness in inhibiting cell proliferation decreases after three weeks on both A2780 and MCF-7 cells. The loss of effectiveness remains almost consistent and stable in a 3-10-weeks range. These results support a limited therapeutic use of this API, due to its poor shelf-life. Therefore, our first endpoint was the increase of this API shelf-life by preventing any protein instability, thus preserving the biological activity.

Since the layer-by-layer fabrication process, is based on the progressive coating of nanoemulsions which is mainly driven by electrostatic forces, the first step to undertake was the ζ- potential measurement of the API. In fact, to achieve nanoassemblies of suitable dimensions and with a narrow size distribution, the polymeric concentric layers should expose

opposite superficial electric charges to allow homogeneous coverage of the NC. We decided to use a 0.985 µM rMnSOD for *in vitro* assay, which is very close to the concentration used by Mancini and co-workers, *i.e.,* 1.5 µM (Mancini et al., 2008). To plan a suitable fabrication strategy, a 0.985 µM rMnSOD solution was tested by DLS and its ζ- potential was found to be positive (+18.23 mV ± 1.01). Therefore, we decided to incorporate the protein in a hyaluronic acid polymeric network, which features negative ζ- potential because of its free carboxyl groups, which are predominantly dissociated at the physiological pH. The size and ζ- potential of the NCs were checked throughout the fabrication process and no significant variation was recorded. The average sizes, polydispersity index (PDI) and ζ -potential are listed in Table 1. The DLS data indicate that the trilayer NCs were fabricated with dimensions that are only slightly above 100 nm, featuring a positive superficial charge and with reasonable PDI. This is relevant as Gonda and co-workers (Gonda et al., 2019) estimated the ideal range of NCs for cancer applications to be within a range of ~10–200 nm. As shown in Figure 2 the progressive coating of the NCs and the inclusion of the protein in the vehicles do not lead to any appreciable modification in their size and morphology. A scheme regarding the fabrication and morphology of NCs is reported in Figure 3.

3.2 Characterization of the formulation

Besides DLS analysis, which is an indirect technique for particle size assessment, as it is based on how particles interplay with a scattered light, the final NCs were morphologically characterized by both cryo-TEM and SEM. TEM provides valuable assets on the inner structure of the sample, such as crystal structure, morphology, and stress state information, while SEM offers insights on the sample's surface and its composition. Moreover, it is important to point out that TEM requires observation of samples cooled to cryogenic temperatures and embedded in an environment of vitreous water, whereas DLS allows observation of sample in the solvated state, in which solvent molecules are associated with the particles. Solvent molecules interact with the particle *via* a variety of non-covalent interactions, *e.g.,* hydrogen bonding, van der Waals interactions, pi-pi stacking. The solvation properties depend upon the solvent chemistry and it is quite common that the particles suspended in different solvents or mixtures thereof exhibit slightly different sizes as recorded by DLS.

As already stated, trilayer NCs had the following composition: lecithin nano emulsion 0.25% (w:w), chitosan-n-acetylcysteine 0.0025% (w:w), a mixture of hyaluronic acid 0.006% (w:w) and rMnSOD 0.0015% (w:w) and an external interface featuring chitosan-n-acetylcysteine 0.009% (w:w). Bilayer NCs featured the same composition except for the external interface, which was not applied.

The SEM images show that the final NCs containing the protein have spheroidal morphology and do not present any noticeable irregularity on their surfaces (Figure 4). Their size seems to be on average of around 100 nm, as recorded by DLS measurements (Figure 3). The comparison with empty trilayer NCs supports that the inclusion of rMnSOD does not result in any evident modification of their morphological structure. This suggests a rather homogeneous packing of the protein into the polymer multilayer nanoassembly.

The cryo-EM images showed electron-dense circular spots clearly attributable to our NCs (Figure 5). These experiments strongly confirmed the spheroidal morphology and revealed a continuous and homogenous build-up of the particles. Their size equalled or fell behind 100 nm and this was consistent in all the sampling sections observed. Furthermore, the sampling sections looked clean and no impurities or free-floating polymer were evident. This is a further indication of the suitability and overall quality of the nanofabrication process.

3.3 Cellular response to rMnSOD formulations *in vitro*

The prepared rMnSOD NCs were then tested for their biological activity on a selected panel of healthy and cancerous cells. We selected the cancerous cell lines MCF-7 (epithelial-like type human breast adenocarcinoma cells), previously used to characterize the *in vitro* activity of rMnSOD (Mancini et al., 2008) and A2780 (human ovarian cancer cells) as *in vitro* models of endocrine responsive cells. Moreover, MCF-10A (human breast epithelial cells) and HaCaT (human keratinocytes) cell lines were used as healthy control cells. The cell viability assay was performed for all tested formulations (empty monolayer, bilayer, trilayer NCs, rMnSOD in aqueous solution and encapsulated rMnSOD in bilayer and trilayer NCs), all stored under the same conditions, *i.e.,* 4°C. The obtained results are reported as “Cell survival index” in Figure 6. The cell viability data for A2780 cell line clearly indicated that freshly empty prepared NCs are safer to use, leading to a low cellular toxicity (12%). After 24 and 30 weeks, a toxicity, no

more than 20%, was observed for the empty NCs. This circumstance may be due to the long-term storage which might have triggered rancidity, oxidation, and peroxide formation, reason why antioxidants are routinely added to oils used in pharmaceutical preparations. Regarding the rMnSOD, its therapeutic effect is completely abolished after only 3 weeks (Figure 1), and even more after 24 and 30 weeks (Figure 6). Nevertheless, concerning the unformulated and formulated rMnSOD, the cytotoxic activity at t_0, resulted enhanced in the bilayer and further promoted in the trilayer NC formulation. However, comparing the effects of rMnSOD in aqueous solution on cellular viability to those of the protein in bilayer and trilayer NCs, the difference becomes striking. Indeed, after 24 and 30 weeks, the formulated protein reduced the cell viability more than the unformulated API, which clearly lost its activity. Both rMnSOD bilayer and trilayer NCs did not lose their efficacy over time, but rather increased it, even if marginally. Between rMnSOD-loaded bilayer and trilayer NCs, the latter exhibit a higher antitumoral activity against the A2780 cell line, most likely due to the supplementary external CT-NAC shell that further protects the protein. These results indicate that when the API is embedded in concentric layer of biocompatible polymers, its antitumoral activity *in vitro* is stronger at t_0 and is preserved after at least 30 weeks.

In MCF-7 human breast cancer cell line, the empty bilayer NCs are less safe than the empty trilayer NCs. This is in agreement with a number of scientific reports, suggesting that carriers exposing anionic interfaces are more likely to induce cytotoxicity (Goodman et al., 2004), although this is still a matter of debate. Nevertheless, cytotoxicity assay indicates that empty trilayer NCs do not impair cell viability to a relevant extent. When the antitumoral activity of the naked rMnSOD is compared to that of the protein formulated in bilayer and trilayer NCs, conclusions analogous to those ones inferred above can be drawn. Indeed, the biocompatible constructs can preserve the antitumoral activity of the protein up to 30 weeks. Although, the rMnSOD bilayer and trilayer NCs seem to reduce the cell viability to a similar extent, trilayer NCs should be preferred due to a less cytotoxicity of the vehicle. The rMnSOD antitumor activity in the trilayer NCs should be considered ≈ 10% stronger. This can be justified by a further shielding that an additional layer could offer.

To evaluate the effects of the formulations on non-cancerous cell lines, the cell viability of non-tumorigenic breast epithelial cell line MCF-10A and in human HaCaT keratinocytes after treatments was assessed, as reporting in Figure 7. Indeed, the antiproliferative effect of

rMnSOD on MCF10A cells was previously evaluated, showing no significant cytotoxic effect. The release of the enzyme lactate dehydrogenase from MCF-10A cells exposed to a 1.5 µM unformulated rMnSOD was only of 10% and growth inhibition was less to 2% after 24 hours, suggesting a very negligible effects on cell viability (Mancini et al., 2006). Analogously to that observed in MCF-7 cells, the bilayer NCs were less safe than the empty trilayer NCs. Nevertheless, the cell survival index never fell below 80% in either cases. Consistently, when the API was included in bilayer NCs, a decrease in cell viability by approximatively 30% was observed. However, the rMnSOD-loaded trilayer NCs exerted a lower *in vitro* effect than the bilayer NCs.

Moreover, when the activity of rMnSOD-loaded trilayer NCs is compared on both breast cells, *i.e.,* MCF-7 and MCF-10A, the cell viability resulted reduced at least to 50% in cancerous cells whereas this was decreased only to 20% in healthy cells. This is consistent with the previous studies performed on the pharmacological activity of rMnSOD (Borrelli et al., 2011; Borrelli et al., 2009) that selectively targets cancerous cells expressing the estrogenic receptor and containing low amount of catalase enzyme.

The formulations were also tested on normal human keratinocytes, HaCaT cell line (Figure 7). Surprisingly, the unformulated rMnSOD caused a slight reduction of cell viability especially at t_0. This was unexpected as the HaCaT cells were selected as a control non-cancerous cell line. However, Frank *et al.* previously reported a cytostatic/antiproliferative effect of Copper/Zinc SOD in human HaCaT keratinocytes (Frank et al., 2000). However, when the API is included in the trilayer NCs, its activity seems weaker, at least when the formulation is freshly prepared. This effect disappeared after 24 and 30 weeks.

4. Concluding remarks

rMnSOD can be an extremely powerful and selective API designed for antitumoral treatment, targeting specifically endocrine responsive cancer cells, such as ovarian and breast cancer cells. However, its use is severely hampered by the remarkable protein instability, due to an interplay of unfolding and aggregation phenomena, which leads the API to be ineffective after

three weeks when stored at 4°C. The incorporation of the protein in concentric alternate layers of chitosan-N-acetylcysteine and hyaluronic acid enhanced the API's effect and selectivity *in vitro* already at time zero, maintaining and extending the efficacy of this anticancer agent even up to 30 weeks when stored at 4°C. The formulation strategy was implemented considering a possible future exploitation of these constructs in animal testing. Due to this, NCs exposing hyaluronic acid interfaces were designed because of the active targeting of CD44, largely expressed by solid tumours. At the same time, chitosan-N-acetylcysteine interfaces provide mucoadhesivity, possibly increasing the residence time of these constructs within the cancerous lesions. The improved activity of rMnSOD loaded NCs could be due the protective action of the vehicle, which probably delay rMnSOD protein denaturation. The results of our investigation broaden the commercial exploitation and clinical applicability of these rMnSOD loaded NCs *in vivo*.

Acknowledgements

Dr. Valentina Mollo is gratefully acknowledged for her support during cryo-EM and SEM experiments. This work was supported by two grants: one from Regione Campania-POR Campania FESR 2014/2020 "Combattere la resistenza tumorale: piattaforma integrata multidisciplinare per un approccio tecnologico innovativo alle oncoterapie-Campania Oncoterapie" (Project N. B61G18000470007) and one fellowship (recipient: GR) PON 03PE_00214_1 "Sperimentazione e studio di tecniche innovative di Imaging con correlazione in ambito chimico farmaceutico", Progetto TECLA; CUP: B72I14000710005.

436

437

438

439

440

441

442

443

444

445

446

447

448

449

450

451

452

453

454

455

456

457

458

Figures

Figure 1.

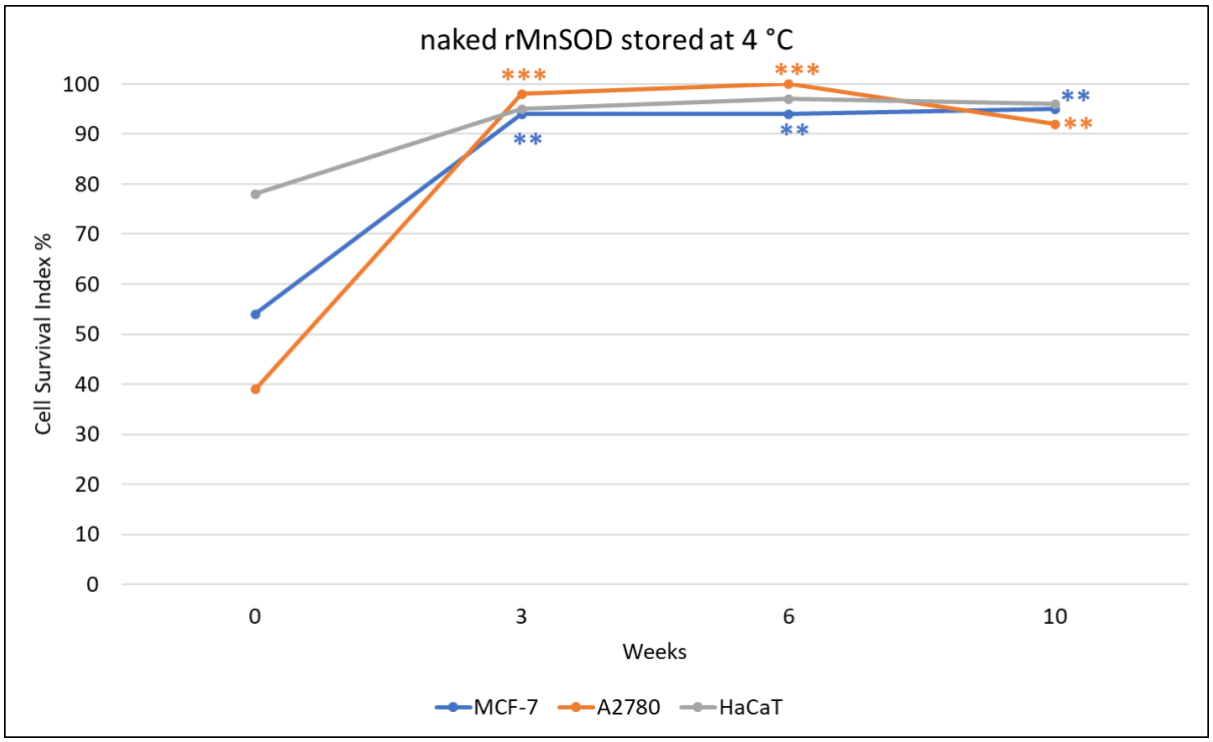

Figure 1. Effects of unformulated rMnSOD (0.985 µM aqueous solution) on MFC-7 (blue), A2780 (orange) and HaCaT (grey) cell viability. Values are expressed as a percentage of untreated control cells and are reported as the mean of five independent experiments ± SEM (n = 30). *** $p < 0.001$ vs. cells treated at t_0; ** $p < 0.01$ vs cells treated at t_0.

Figure 2.

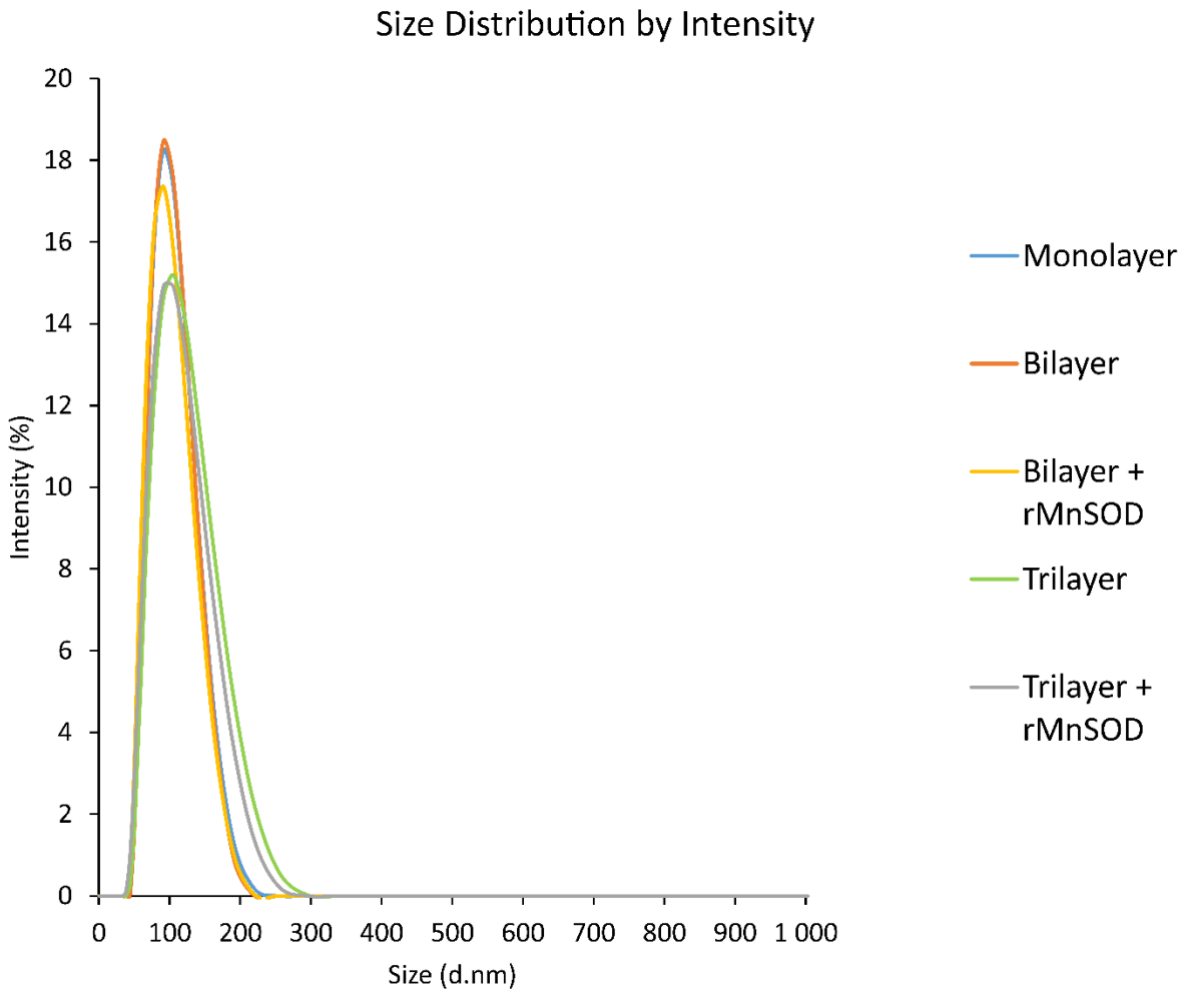

Figure 2. Size distribution (nm in diameter) by intensity measured by Dynamic Light Scattering of monolayer (blue), bilayer (orange), trilayer (green), bilayer + rMnSOD (yellow) and trilayer + rMnSOD (grey).

Figure 3.

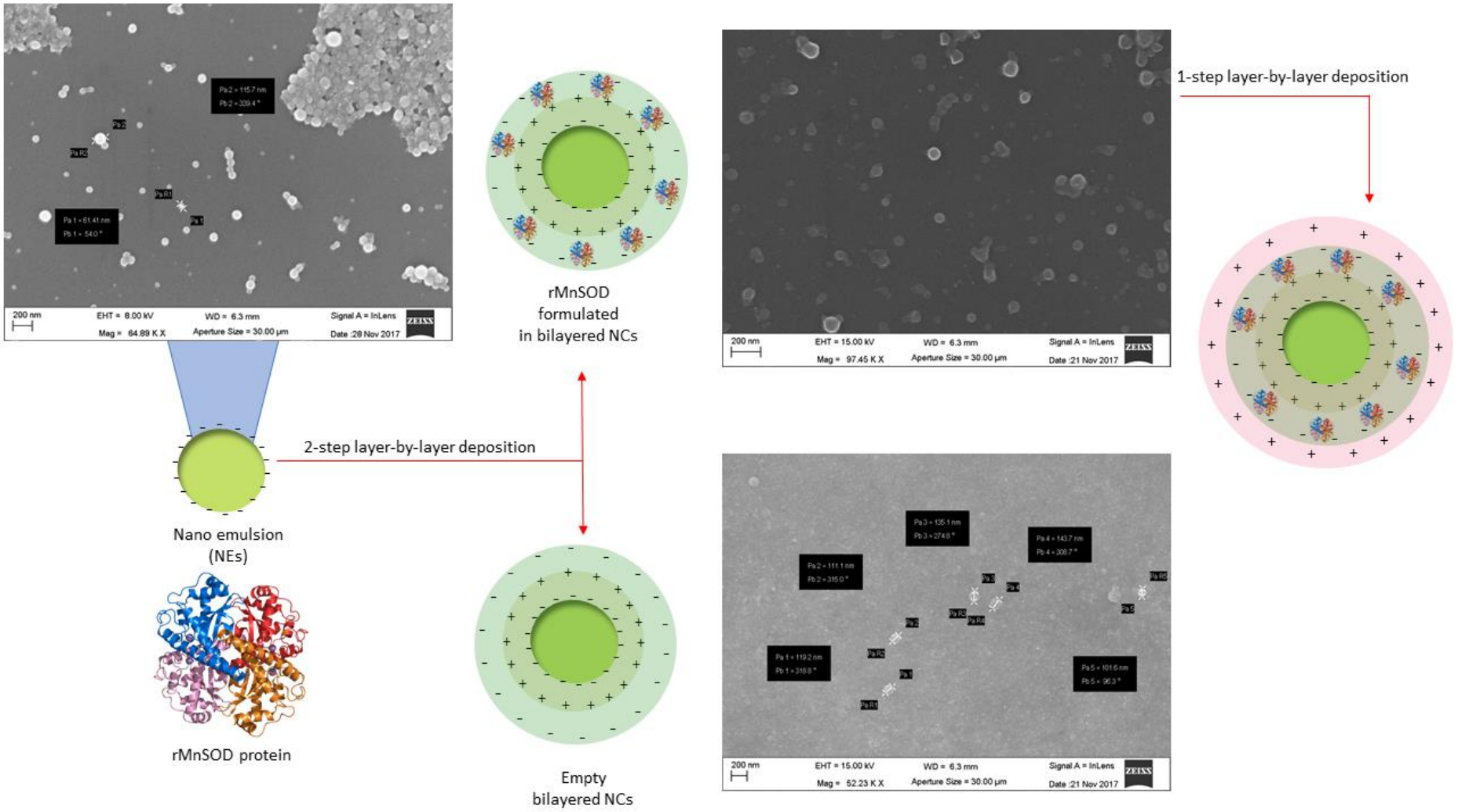

Figure 3. Exemplative scheme describing the fabrication and morphology of nanoemulsion droplets, empty bilayer and rMnSOD bilayer NCs.

Figure 4.

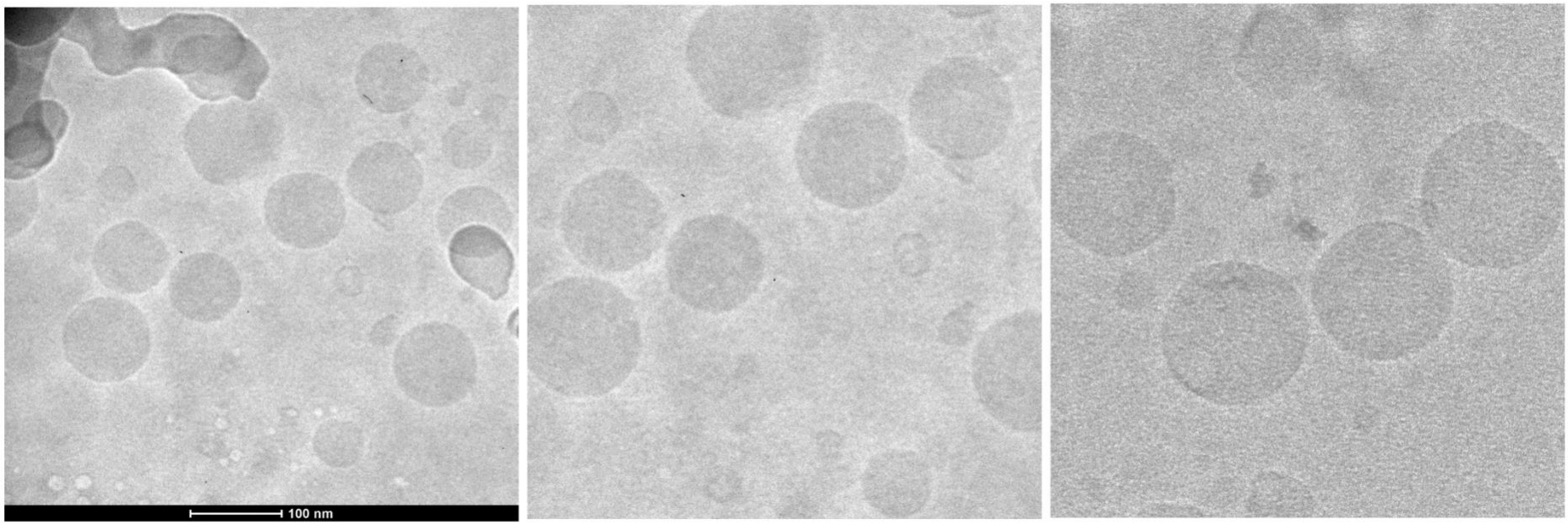

Figure 4. Cryo-EM images of rMnSOD trilayer NCs. The composition of these NCs is covered in 2.1.1.3, the experimental details for the imagining is described in 2.1.2.4.

494 **Figure 5.**

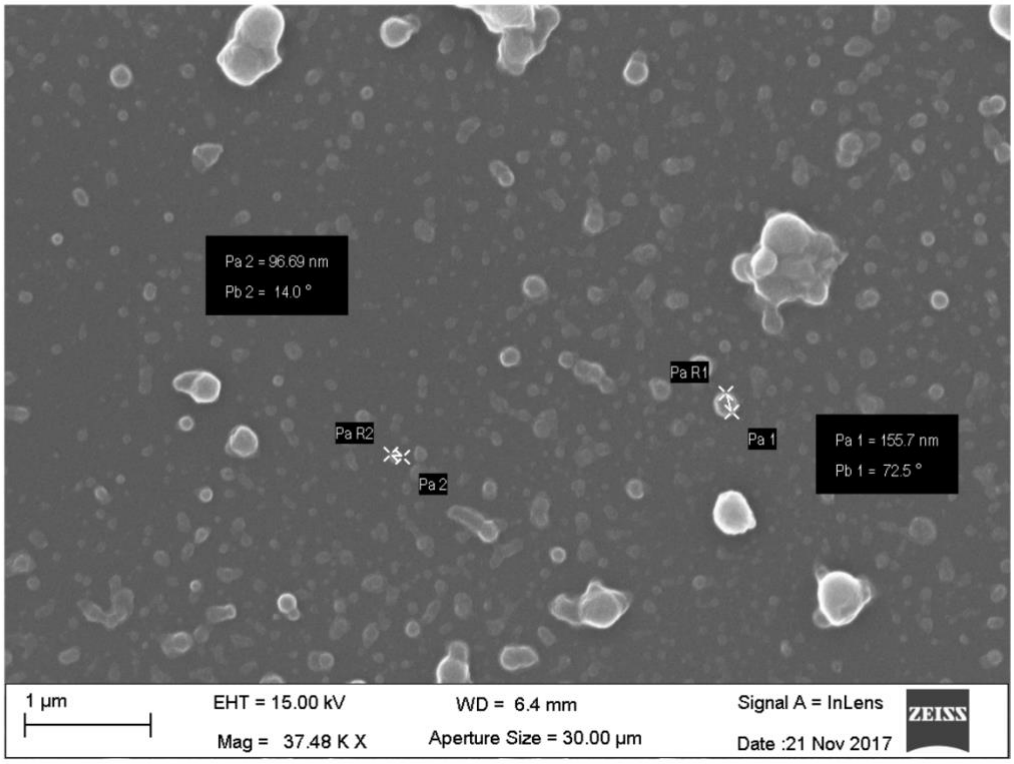

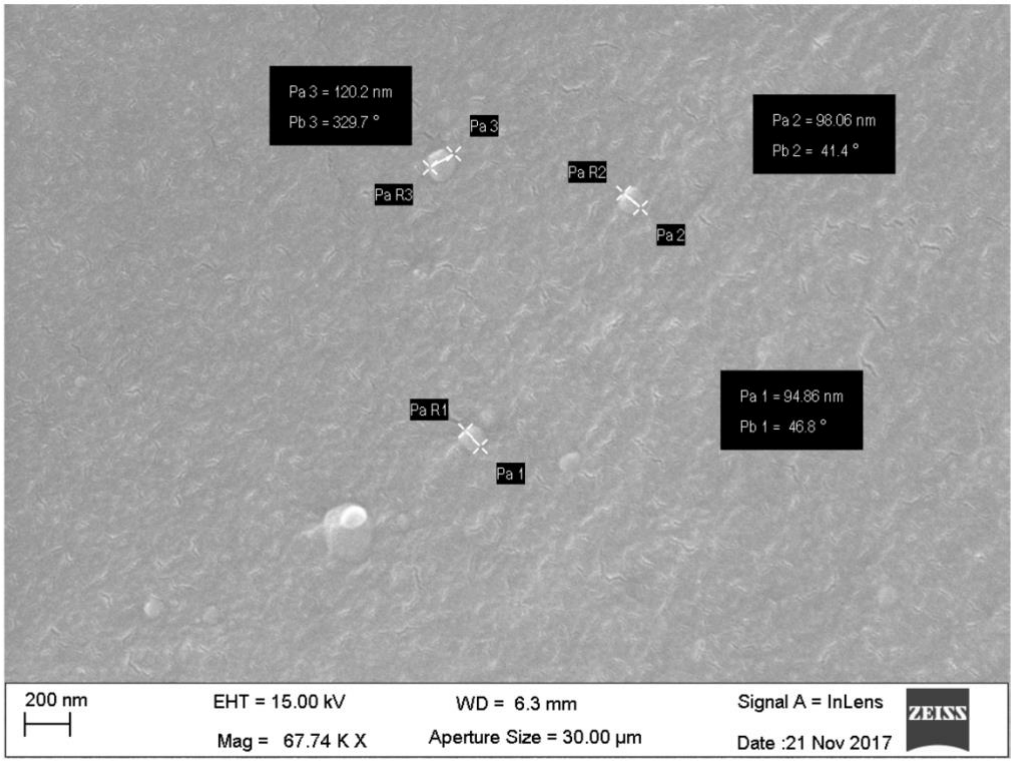

495

Figure 5. SEM images of rMnSOD trilayer assemblies. The composition of these NCs is covered in 2.1.1.3, the experimental details for the imagining is described in 2.1.2.5.

Figure 6.

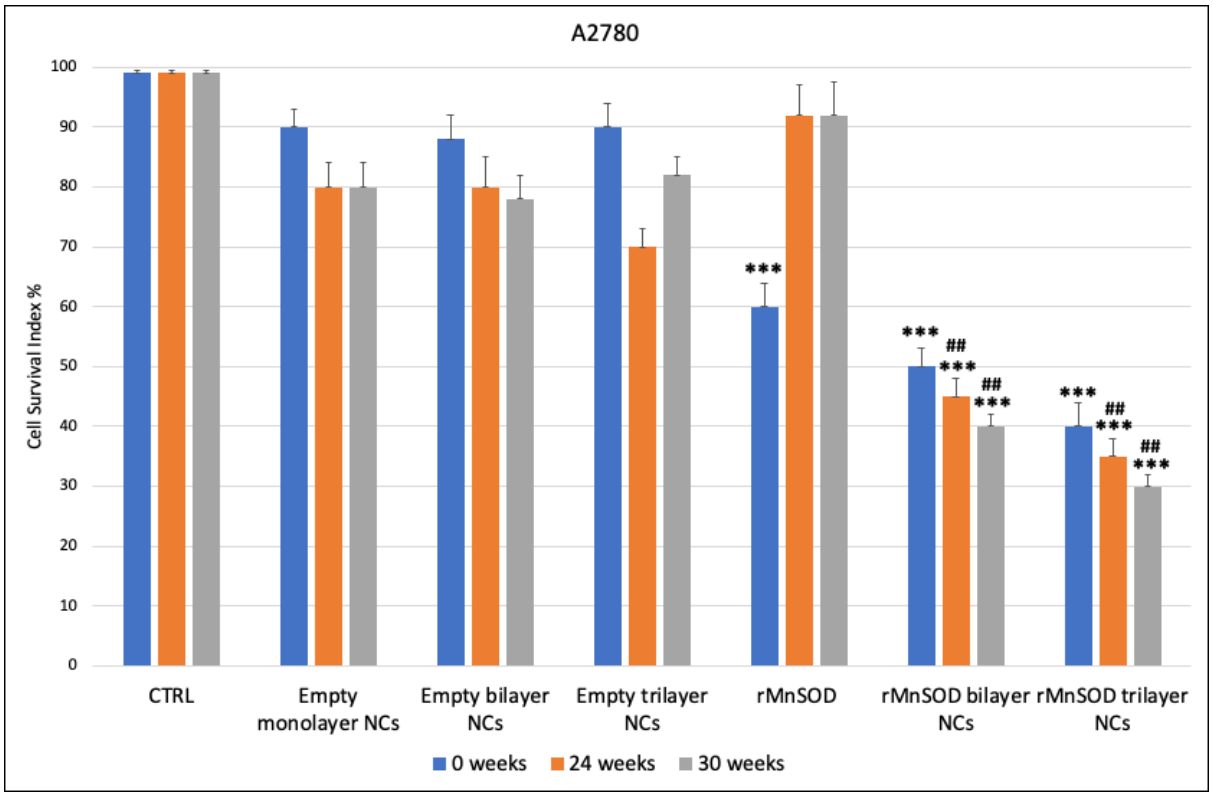

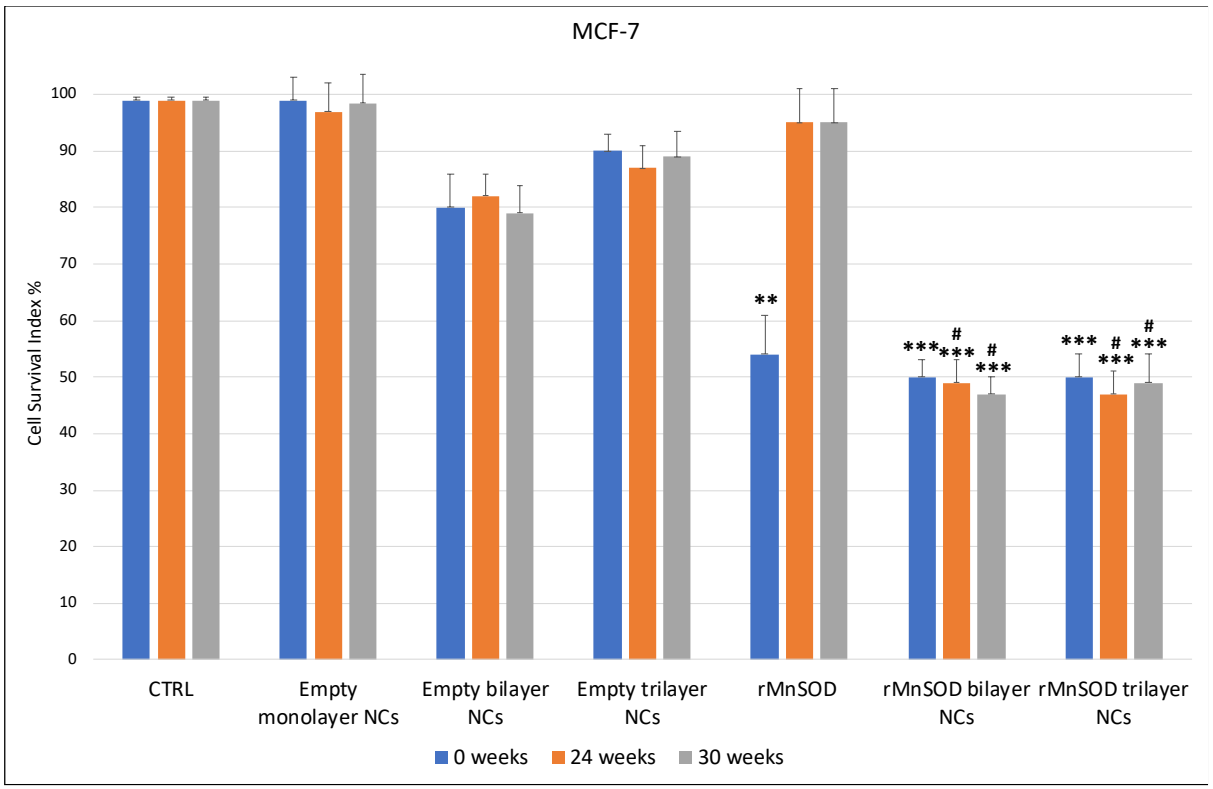

Figure 6. Bioscreen for cellular responses to rMnSOD formulations *in vitro*. Cell survival index, evaluated by the MTT assay and live/dead cell ratio, for cancerous cell lines, A2780 and MCF-7, following treatment with empty monolayer, empty bilayer, empty trilayer NCs, 0.985 µM

rMnSOD in aqueous solution and 0.985 µM rMnSOD incorporated in bilayer and trilayer NCs at time 0 (blue), after 24 weeks (orange) and 30 weeks (grey). Values are expressed as a percentage of untreated control cells and are reported as the mean of five independent experiments ± SEM (n = 30). *** $p < 0.001$ vs. control; ** $p < 0.01$ vs.control; $^{\#}$ $p < 0.05$ vs rMnSOD; $^{\#\#}$ $p < 0.01$ vs rMnSOD.

Figure 7.

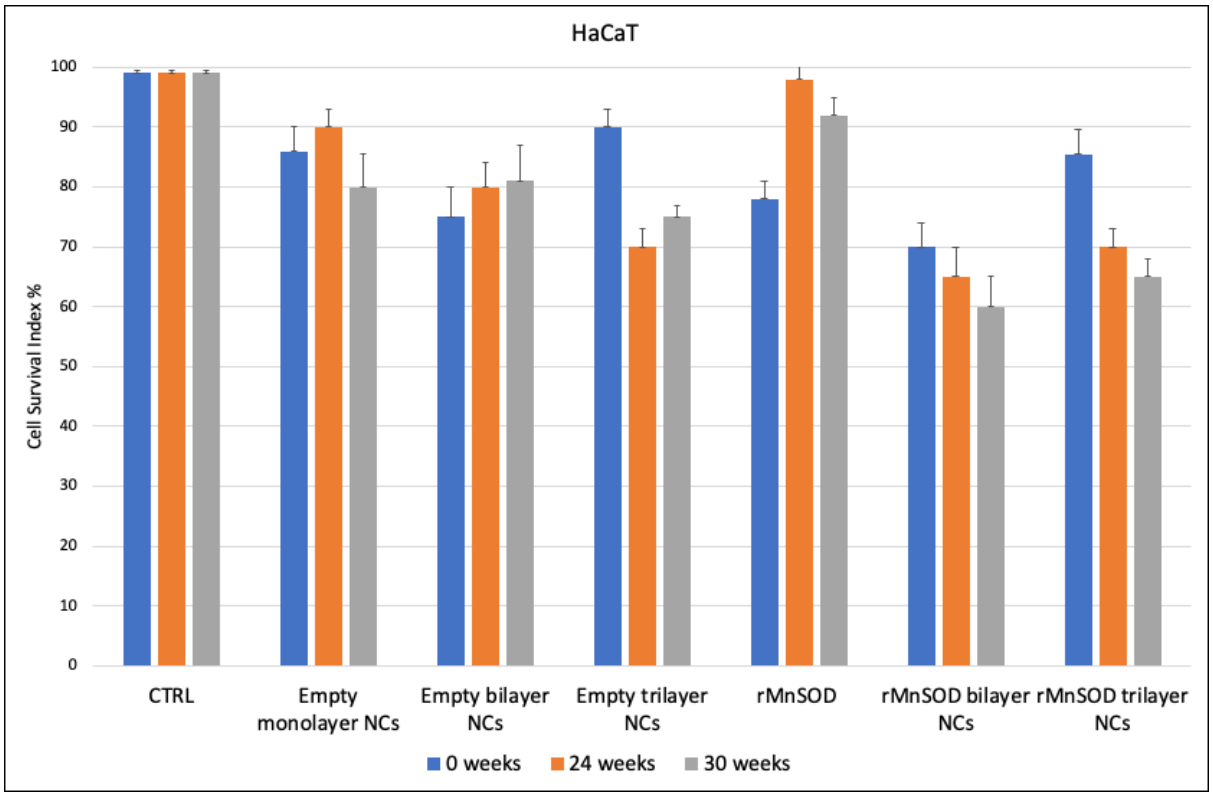

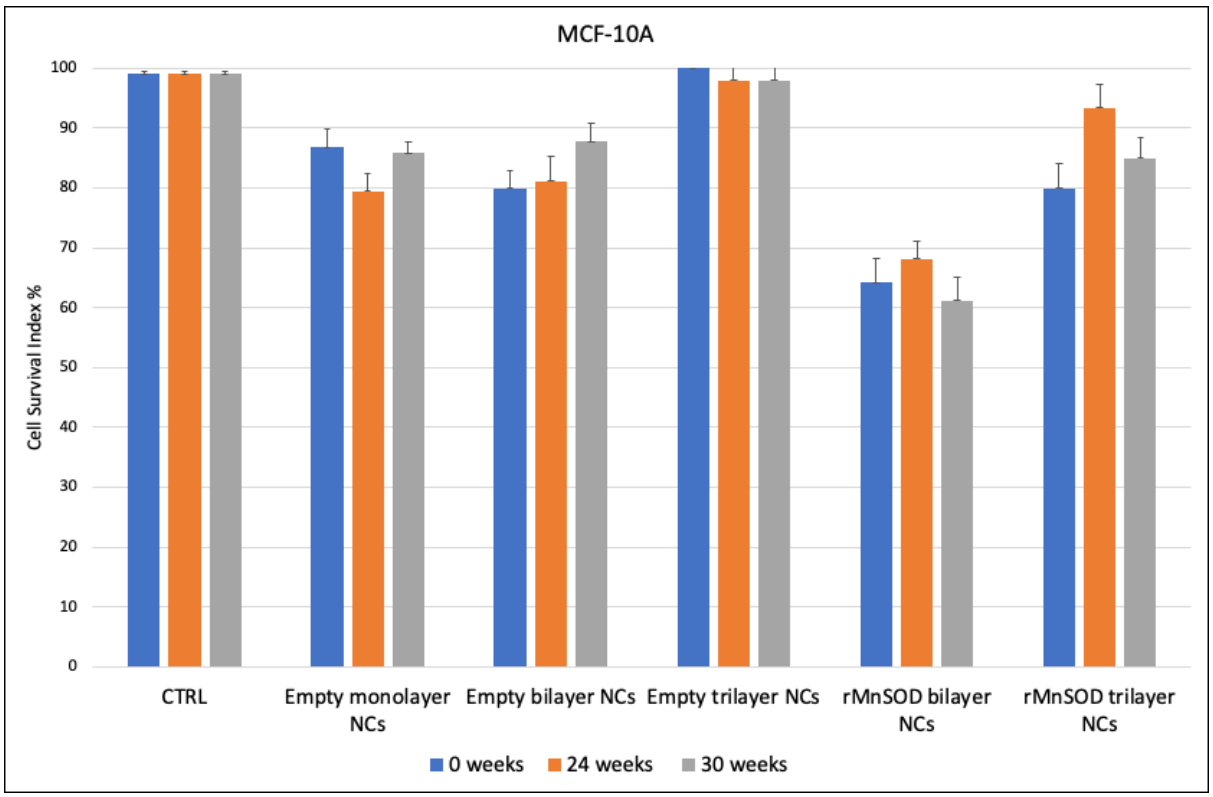

Figure 7. Bioscreen for cellular responses to rMnSOD formulations in vitro. Cell survival index for non-cancerous cell lines HaCaT and MCF-10A, following treatment with empty monolayer, empty bilayer, empty trilayer NCs, 0.985 µM rMnSOD in aqueous solution and 0.985 µM

535 rMnSOD incorporated in bilayer and trilayer NCs at time 0 (blue), after 24 weeks (orange) and
536 30 weeks (grey). Values are expressed as a percentage of untreated control cells and are
537 reported as the mean of five independent experiments ± SEM (n = 30). Data were not
538 statistically significant.

Table 1.

Sample	Size (nm)	ζ- potential (mV)	PDI
Monolayer	**104.0**	**+15.04 ± 3.1**	**0.127**
Bilayer	**106.1**	**-28.80 ± 4.6**	**0.163**
Trilayer	**105.3**	**+18.61 ± 3.7**	**0.133**

Table 1. Average of Size (nm), zeta-potential (mV) and PDI for the main products of layer-by-layer deposition.

References

Borrelli, A., Schiattarella, A., Mancini, R., Morelli, F., Capasso, C., De Luca, V., Gori, E., Mancini, A., 2011. The leader peptide of a human rec. MnSOD as molecular carrier which delivers high amounts of Cisplatin into tumor cells inducing a fast apoptosis in vitro. Int J Cancer 128, 453-459.

Borrelli, A., Schiattarella, A., Mancini, R., Morrica, B., Cerciello, V., Mormile, M., d'Alesio, V., Bottalico, L., Morelli, F., D'Armiento, M., D'Armiento, F.P., Mancini, A., 2009. A recombinant MnSOD is radioprotective for normal cells and radiosensitizing for tumor cells. Free Radic Biol Med 46, 110-116.

Borrelli, A., Schiattarella, A., Mancini, R., Pica, A., Pollio, M.L., Ruggiero, M.G., Bonelli, P., De Luca, V., Tuccillo, F.M., Capasso, C., Gori, E., Sanseverino, M., Carpentieri, A., Birolo, L., Pucci, P., Rommelaere, J., Mancini, A., 2016. A new hexapeptide from the leader peptide of rMnSOD enters cells through the oestrogen receptor to deliver therapeutic molecules. Sci Rep 6, 18691.

Ceelen, W.P., Flessner, M.F., 2010. Intraperitoneal therapy for peritoneal tumors: biophysics and clinical evidence. Nat Rev Clin Oncol 7, 108-115.

Damiano, S., Trepiccione, F., Ciarcia, R., Scanni, R., Spagnuolo, M., Manco, L., Borrelli, A., Capasso, C., Mancini, R., Schiattarella, A., Iervolino, A., Zacchia, E., Bata-Csere, A., Florio, S., Anastasio, P., Pollastro, R., Mancini, A., Capasso, G., 2013. A new recombinant MnSOD prevents the cyclosporine A-induced renal impairment. Nephrol Dial Transplant 28, 2066-2072.

Folz, R.J., Guan, J., Seldin, M.F., Oury, T.D., Enghild, J.J., Crapo, J.D., 1997. Mouse extracellular superoxide dismutase: primary structure, tissue-specific gene expression, chromosomal localization, and lung in situ hybridization. Am J Respir Cell Mol Biol 17, 393-403.

Frank, S., Kampfer, H., Podda, M., Kaufmann, R., Pfeilschifter, J., 2000. Identification of copper/zinc superoxide dismutase as a nitric oxide-regulated gene in human (HaCaT) keratinocytes: implications for keratinocyte proliferation. Biochem J 346 Pt 3, 719-728.

Gonda, A., Zhao, N., Shah, J.V., Calvelli, H.R., Kantamneni, H., Francis, N.L., Ganapathy, V., 2019. Engineering Tumor-Targeting Nanoparticles as Vehicles for Precision Nanomedicine. Med One 4.

Goodman, C.M., McCusker, C.D., Yilmaz, T., Rotello, V.M., 2004. Toxicity of Gold Nanoparticles Functionalized with Cationic and Anionic Side Chains. Bioconjugate Chemistry 15, 897-900.

Greenlee, R.T., Murray, T., Bolden, S., Wingo, P.A., 2000. Cancer statistics, 2000. CA Cancer J Clin 50, 7-33.

Grumetto, L., Del Prete, A., Ortosecco, G., Barbato, F., Del Prete, S., Borrelli, A., Schiattarella, A., Mancini, R., Mancini, A., 2015. Study on the Protective Effect of a New Manganese Superoxide Dismutase on the Microvilli of Rabbit Eyes Exposed to UV Radiation. Biomed Res Int 2015, 973197.

Holley, A.K., Bakthavatchalu, V., Velez-Roman, J.M., St Clair, D.K., 2011. Manganese superoxide dismutase: guardian of the powerhouse. Int J Mol Sci 12, 7114-7162.

Krause, M.E., Sahin, E., 2019. Chemical and physical instabilities in manufacturing and storage of therapeutic proteins. Curr Opin Biotechnol 60, 159-167.

Mancini, A., Borrelli, A., Schiattarella, A., Aloj, L., Aurilio, M., Morelli, F., Pica, A., Occhiello, A., Lorizio, R., Mancini, R., Sica, A., Mazzarella, L., Sica, F., Grieco, P., Novellino, E., Pagnozzi, D., Pucci, P., Rommelaere, J., 2008. Biophysical and biochemical characterization of a liposarcoma-derived recombinant MnSOD protein acting as an anticancer agent. Int J Cancer 123, 2684-2695.

Mancini, A., Borrelli, A., Schiattarella, A., Fasano, S., Occhiello, A., Pica, A., Sehr, P., Tommasino, M., Nuesch, J.P., Rommelaere, J., 2006. Tumor suppressive activity of a variant isoform of manganese superoxide dismutase released by a human liposarcoma cell line. Int J Cancer 119, 932-943.

Momenimovahed, Z., Tiznobaik, A., Taheri, S., Salehiniya, H., 2019. Ovarian cancer in the world: epidemiology and risk factors. Int J Womens Health 11, 287-299.

Piccolo, M., Ferraro, M.G., Maione, F., Maisto, M., Stornaiuolo, M., Tenore, G.C., Santamaria, R., Irace, C., Novellino, E., 2019a. Induction of Hair Keratins Expression by an Annurca Apple-Based Nutraceutical Formulation in Human Follicular Cells. Nutrients 11.

Piccolo, M., Misso, G., Ferraro, M.G., Riccardi, C., Capuozzo, A., Zarone, M.R., Maione, F., Trifuoggi, M., Stiuso, P., D'Errico, G., Caraglia, M., Paduano, L., Montesarchio, D., Irace, C., Santamaria, R., 2019b.

Exploring cellular uptake, accumulation and mechanism of action of a cationic Ru-based nanosystem in human preclinical models of breast cancer. Sci Rep 9, 7006.
Stetefeld, J., McKenna, S.A., Patel, T.R., 2016. Dynamic light scattering: a practical guide and applications in biomedical sciences. Biophys Rev 8, 409-427.
Vecchione, R., Ciotola, U., Sagliano, A., Bianchini, P., Diaspro, A., Netti, P.A., 2014. Tunable stability of monodisperse secondary O/W nano-emulsions. Nanoscale 6, 9300-9307.
Vecchione, R., Iaccarino, G., Bianchini, P., Marotta, R., D'Autilia, F., Quagliariello, V., Diaspro, A., Netti, P.A., 2016. Ultrastable Liquid-Liquid Interface as Viable Route for Controlled Deposition of Biodegradable Polymer Nanocapsules. Small 12, 3005-3013.
Wan, X.S., Devalaraja, M.N., St Clair, D.K., 1994. Molecular structure and organization of the human manganese superoxide dismutase gene. DNA Cell Biol 13, 1127-1136.
Ye, H., Tanenbaum, L.M., Na, Y.J., Mantzavinou, A., Fulci, G., del Carmen, M.G., Birrer, M.J., Cima, M.J., 2015. Sustained, low-dose intraperitoneal cisplatin improves treatment outcome in ovarian cancer mouse models. J Control Release 220, 358-367.
Zhidkov, N., De Souza, R., Ghassemi, A.H., Allen, C., Piquette-Miller, M., 2013. Continuous intraperitoneal carboplatin delivery for the treatment of late-stage ovarian cancer. Mol Pharm 10, 3315-3322.